

# Estimating wall-shear-stress fluctuations given an outer region input

Romain Mathis<sup>1,2,†</sup>, Ivan Marusic<sup>1</sup>, Sergei I. Chernyshenko<sup>3</sup>  
and Nicholas Hutchins<sup>1</sup>

<sup>1</sup>Department of Mechanical Engineering, University of Melbourne, Victoria 3010, Australia

<sup>2</sup>Laboratoire de Mécanique de Lille, UMR CNRS 8107, 59655 Villeneuve d'Ascq, France

<sup>3</sup>Department of Aeronautics, Imperial College, London SW7 2AZ, UK

(Received 14 May 2012; revised 31 August 2012; accepted 10 October 2012)

A model for the instantaneous wall-shear-stress distribution is presented for zero-pressure-gradient turbulent boundary layers. The model, based on empirical and theoretical considerations, is able to reconstruct a statistically representative fluctuating wall-shear-stress time-series,  $\tau_w'(t)$ , using only the low-frequency content of the streamwise velocity measured in the logarithmic region, away from the wall. Results, including spectra and second-order moments, show that the model is capable of successfully capturing Reynolds number trends as observed in other studies.

**Key words:** turbulent boundary layers, turbulent flows

## 1. Introduction

A key defining parameter for wall-bounded flows is the wall shear stress,  $\tau_w$ . The mean, time-averaged, value  $\bar{\tau}_w$  has been extensively investigated both theoretically and experimentally, and is often expressed as a friction velocity,  $U_\tau = \sqrt{\bar{\tau}_w/\rho}$  (where  $\rho$  is the fluid density), which has been used as the scaling velocity in boundary layer analyses going back to Prandtl (1905). Various empirical/semi-theoretical formulations have been proposed for how  $\bar{\tau}_w$  varies with Reynolds number including those of Kármán–Schoenherr (Schlichting & Gersten 2000), Coles–Fernholz (Fernholz & Finley 1996), and Monkewitz, Chauhan & Nagib (2007), amongst others.

Far less is known about the fluctuating component of wall-shear stress,  $\tau_w'$ , where

$$\tau_w'(\mathbf{x}, t) = \tau_w(\mathbf{x}, t) - \bar{\tau}_w(\mathbf{x}) \quad (1.1)$$

and how its statistics change with Reynolds number. In classical scaling approaches that assume the law of the wall (see Smits, McKeon & Marusic 2011a) the statistics of  $\tau_w'^+ = \tau_w'/\bar{\tau}_w$  are invariant with Reynolds numbers. However, it has been shown in laboratory (Alfredsson *et al.* 1988; Marusic & Heuer 2007) and numerical simulation (Örlü & Schlatter 2011) studies of wall-bounded flows that Reynolds number effects do exist, and very large instantaneous values of wall shear can occur well above the mean values. For example, the maximum of the instantaneous fluctuating wall shear stress can exceed five times the mean value (see figure 3 of Örlü & Schlatter 2011),

† Email address for correspondence: [rmathis@unimelb.edu.au](mailto:rmathis@unimelb.edu.au)

and such events occur more frequently as the Reynolds number increases (Klewicki 2010; Lenaers *et al.* 2012). Such large excursions can be important in a range of applications where scouring and mechanical damage can result because of excessive levels of instantaneous shear stress. In environmental flows, such as in rivers and streams, the fluctuating wall shear stress is of significant ecological importance, as it is linked to erosion, bed formation, sediment transportation, interfacial gas and nutrient transport, etc. (Grant & Madsen 1986; Rowiński, Aberle & Mazurczyk 2005; Grant & Marusic 2012).

From an experimental point of view, direct measurement of the instantaneous wall-shear-stress distribution is challenging as it requires a non-intrusive method applied at or very close to the wall (Chew *et al.* 1998). These difficulties are compounded in high-Reynolds-number flows where spatial and temporal resolution effects become prohibitive (Hutchins *et al.* 2009; Smits *et al.* 2011*b*). Direct numerical simulations (DNS) can overcome these problems, but remain limited, even nowadays, to low Reynolds numbers. Consequently, there is a significant lack of knowledge of the Reynolds number ( $Re$ ) dependence of  $\tau_w$ , particularly at high  $Re$ . Several methods have been developed to palliate these issues and provide estimates of the wall shear stress (however only in the mean sense). For example, in zero-pressure-gradient smooth-wall flows, the law of the wall and the Reynolds-stress method are commonly used, and have proven to be reasonably accurate (Chauhan, Ng & Marusic 2010). However, these methods become less accurate in other flow configurations such as rough walls, complex geometries, or in the presence of emergent vegetation (see Rowiński *et al.* 2005, for a review of the main methods available for the evaluation of the skin friction). Despite the known errors, these methods remain widely used in environmental flows (Brand *et al.* 2010), because they are currently the only way to estimate the skin friction. In an attempt to address this, herein we propose an empirical model that is capable of reconstructing the instantaneous distribution of the wall shear stress based on inner–outer interactions.

In wall-bounded turbulent flows, it is now well established that the near-wall region (where viscous wall scaling alone applies for the mean flow, typically taken to be below the logarithmic region) is not independent of motions in the outer region (taken to be the logarithmic region and above), and in fact the interactions can be quite strong. Large- and very-large-scale motions have been observed to develop in the outer layer (Kim & Adrian 1999; del Álamo & Jiménez 2003; Tomkins & Adrian 2003; Hambleton, Hutchins & Marusic 2006; Hutchins & Marusic 2007*a*, amongst others), in all types of wall-bounded flows (Monty *et al.* 2007; Marusic & Hutchins 2008). These large-scale events have been shown to be dependent on changes in Reynolds number, becoming more energetic and prominent as  $Re$  increases (Hutchins & Marusic 2007*a*). Particularly, it has been put forward that these events influence significantly the near-wall flow, by means of superposition and amplitude modulation effects (Bandyopadhyay & Hussain 1984; Grinvald & Nikora 1988; Hutchins & Marusic 2007*b*; Mathis *et al.* 2009*b*, 2011*b*; Chung & McKeon 2010). Brown & Thomas (1977) have previously reported the influence of the outer region onto the wall shear stress by clearly identifying a large-scale superposition effect, and this is supported by Örlü & Schlatter (2011) who, through DNS, documented the low-wavenumber changes in the two-dimensional spectra map of wall shear stress (see their figure 4).

Other mechanisms for the inner–outer interactions have been described in the literature, and further work is needed to firmly establish how these relate to superposition and modulation effects. The superposition component is directly related to the attached eddy hypothesis (Townsend 1976; Perry & Marusic 1995), and

similarly to the effect of large inactive eddies generated in the interior of the boundary layer whose vorticity has an impact on the high-shear region near the wall (Hunt & Morrison 2000). The inferred amplitude modulation effect is a nonlinear process and its effects are also probably consistent with a description of wall turbulence in terms of an interacting range of scales of attached packets of eddies. There is some evidence that these packets of eddies can be organized into very-large-scale motions (Kim & Adrian 1999; Adrian, Meinhart & Tomkins 2000; Dennis & Nickels 2011*a,b*), which produce large-scale variations in wall shear stress (Hutchins *et al.* 2011). A related kinematic representation of this is to consider the turbulence in terms of internal shear layers (Hunt *et al.* 2010), and interactions can be considered in terms of blocking and the shear sheltering mechanism reported by Jacobs & Durbin (1998) and Hunt & Durbin (1999). Here, the larger positive outer fluctuations are able to break down the shear (sheltering) layer and penetrate into the buffer layer. This induces high stresses and high skewness at the wall, increasing with Reynolds number (Ptasinski *et al.* 2003; Zaki & Saha 2009), effects which are respectively similar to those induced by superposition and amplitude modulation (Mathis, Hutchins & Marusic 2011*a*). Further discussions of recent advances in wall-bounded turbulent flows, including inner–outer interactions, are given in the recent reviews by Klewicki (2010), Marusic *et al.* (2010*c*), Marusic, Mathis & Hutchins (2010*a*) and Smits *et al.* (2011*a*).

By directly applying the observations of superposition and modulation of the large-scale motions on the small, Marusic, Mathis & Hutchins (2010*b*) developed an empirical model that is able to reconstruct the streamwise velocity field in the near-wall region of the zero-pressure-gradient turbulent boundary layer. The model predicts profiles of representative fluctuating streamwise velocity signals within the inner layer, given only the information of a single point of the large-scale fluctuation in the log region. The formulation models both the superposition and modulation effects imposed by the large scales on the near-wall region. The underlying idea is that the near-wall small-scale motions are universal, i.e. they do not change with Reynolds number. However, these small-scale motions are influenced by large-scale log-region events and the intensity of the influence increases with Reynolds number. Therefore, the Reynolds number effects are confined to the large-scale log-region signal. The model's formulation involves, at each wall-normal position, a universal signal and universal parameters, which are determined from a one-off calibration experiment at an arbitrarily chosen Reynolds number, and are assumed to be independent of Reynolds number. The model has been shown to work very well over a large range of Reynolds numbers, and also to be potentially applicable to other wall-bounded flows such as internal flows (pipes and channels) and turbulent boundary layers subjected to a streamwise pressure gradient (Mathis *et al.* 2011*a*).

In this paper, we extend the approach of Marusic *et al.* (2010*b*) to develop a predictive model that enables us to reconstruct the fluctuating wall-shear stress when only large-scale information from the logarithmic region is known. Using a Taylor's series expansion for the modulated wall shear stress, we are able to reduce the number of parameters in the model, and we describe the calibration procedure for determining the remaining universal parameters. It should be noted that in this paper, the fluctuating wall shear stress refers only to the streamwise component of the total wall shear stress, which is the component contributing to the skin friction coefficient  $C_f$ .

## 2. Wall-shear-stress model

Marusic *et al.* (2010b) and Mathis *et al.* (2011a) provide full details of the model for the streamwise fluctuating velocity signal. We start with this model here and apply it in the viscous sub-layer, where a linear relationship between the streamwise velocity component and the wall shear stress is known. By dividing the formulation for the streamwise fluctuations (equation (1) Marusic *et al.* 2010b) by  $z^+$  we get

$$\tau_{wp}^{\prime+}(t^+) = \tau_w^{\prime*}(t^+)\{1 + \beta u_{OL}^{\prime+}(t^+)\} + \alpha u_{OL}^{\prime+}(t^+), \quad (2.1)$$

where  $\tau_{wp}^{\prime+}$  is the predicted time-series normalized by wall variables,  $\tau_{wp}^{\prime+} = \tau_{wp}'/(\rho U_\tau^2)$  and  $t^+ = tU_\tau^2/\nu$ . (A preliminary version of (2.1) was reported by Marusic, Mathis & Hutchins 2011.) The time-series  $\tau_w^{\prime*}$ , which is normalized in wall units, represents the statistically ‘universal’ wall-shear-stress signal that would exist in the absence of any inner–outer interactions. Here,  $\alpha$  and  $\beta$  are the superposition and modulation coefficients. The subscript  $O$  refers to a signal from an outer location (log-region), and the subscript  $L$  refers to a filtered large-scale component. It should be noted that  $\alpha$  in (2.1) is essentially  $\alpha/z^+$  from Marusic *et al.* (2010b). (Note that the definition of  $\alpha$  in Mathis *et al.* 2011a is not strictly correct and should be modified to include the ratio of the r.m.s., i.e.  $\alpha = \max(R_{u_L^+ u_{OL}^+}) \times (u_L^+)_{rms} / (u_{OL}^+)_{rms}$ .) The parameters  $\tau_w^{\prime*}$ ,  $\alpha$  and  $\beta$  are determined experimentally (described in §4), and are hypothesized to be Reynolds-number independent. Once these parameters are known, the only user input required for the model is a characteristic signal of the large scales from the log region,  $u_{OL}^{\prime+}$ . It is noted that the model consists of two parts. The first part in (2.1) models the amplitude modulation of the small scales, here  $\tau_w^{\prime*}$ , by the large-scale log-region motions,  $u_{OL}^{\prime+}$ . The second term,  $\alpha u_{OL}^{\prime+}$ , models the superposition of the large scales felt at the wall.

The required input for the model, the large-scale signal  $u_{OL}^{\prime+}$ , is obtained from a fluctuating streamwise velocity  $u$ -signal measured, following Mathis, Hutchins & Marusic (2009a), at the approximate geometric centre of the logarithmic layer,  $z_0^+ = 3.9Re_\tau^{1/2}$ . The raw  $u$  signal is first high-pass filtered to retain only the large-scale components, and a spatial shift is applied to take into consideration the inclination angle of the large-scale structures.

## 3. Details of experiments

In order to calibrate and validate the model, we use a series of datasets obtained in the high-Reynolds-number boundary layer wind tunnel at the University of Melbourne. The facility is an open-return blower wind tunnel with a working test section of 27 m  $\times$  2 m  $\times$  1 m. Along the test section, the free-stream turbulence intensity is less than 0.05% and a zero pressure gradient is maintained by bleeding air through the ceiling via adjustable spanwise slots. See Nickels *et al.* (2005) for a more detailed description of the facility.

Measurements of the streamwise velocity component have been made using hot-wire anemometry. The single normal probes used are made from platinum Wollaston wire of various diameters ( $d = 1.5, 2.5$  or  $5 \mu\text{m}$ ). For each experiment, the etched length of the wire,  $l$ , was adjusted to maintain a constant ratio  $l/d \geq 200$ , as recommended by Ligrani & Bradshaw (1987) and Hutchins *et al.* (2009). Close attention has been paid to the choice of the frequency and sampling duration for each experiment in order to properly resolve the small-scale energy content as well as the large-scale structures. A summary of the experimental conditions is given in tables 1 and 2. A composite velocity profile fit (Monkewitz, Chauhan & Nagib 2008) was used to

$Re_\tau$	Facility	$x$ (m)	$U_\infty$ (m s <sup>-1</sup> )	$\delta$ (m)	$U_\tau$ (m s <sup>-1</sup> )	$\nu/U_\tau$ ( $\mu\text{m}$ )	$l^+$	$l/d$	$t_s^+$	$TU_\infty/\delta$
4480	Melbourne	12.80	10.17	0.195	0.350	43.5	11.5	200	0.16	46 900

TABLE 1. Experimental parameters for two-point synchronized hot-wire measurements used for the calibration;  $x$  refers to the distance between the tripped inlet and the measurements station;  $t_s$  is the time between samples; and  $T$  is the total sampling time.

$Re_\tau$	Facility	$x$ (m)	$U_\infty$ (m s <sup>-1</sup> )	$\delta$ (m)	$U_\tau$ (m s <sup>-1</sup> )	$\nu/U_\tau$ ( $\mu\text{m}$ )	$l^+$	$l/d$	$t_s^+$	$TU_\infty/\delta$
2740	Melbourne	1.60	20.12	0.058	0.737	21.1	25.5	354	0.53	26 390
3514	Melbourne	2.65	20.12	0.075	0.726	21.4	25.1	354	0.52	20 271
4228	Melbourne	3.75	20.20	0.092	0.714	21.8	24.8	354	0.50	21 845
5885	Melbourne	6.30	20.12	0.133	0.691	22.5	23.9	354	0.47	19 246
8159	Melbourne	10.00	20.52	0.187	0.686	22.9	23.6	354	0.46	16 351
10 111	Melbourne	12.80	19.95	0.235	0.661	23.2	23.2	354	0.44	19 932
13 320	Melbourne	18.90	19.98	0.322	0.641	22.3	22.3	208	0.41	14 697
17 775	Melbourne	17.95	30.00	0.306	0.934	17.2	29.0	200	0.54	11 776
22 884	Melbourne	17.95	40.70	0.296	1.247	12.9	38.6	200	0.96	13 752
$1.4 \times 10^6$	SLTEST	—	—	$\sim 100$	0.260	69.2	—	—	75.10	$\sim 180$

TABLE 2. Experimental parameters for datasets used for validation; Melbourne experiments were conducted with a single hot-wire probe; SLTEST data were acquired with sonic anemometers.

determine the friction velocity  $U_\tau$  and the boundary layer thickness  $\delta$ , using the log-law constants  $\kappa = 0.384$  and  $A = 4.17$ . The results for  $U_\tau$  are in good agreement with oil-film interferometry measurements performed by Chauhan *et al.* (2010).

The first dataset, given in table 1, is used to calibrate the model. It consists of two-point simultaneous measurements with a wall probe mounted at about one viscous wall unit above the wall ( $z = 45 \mu\text{m}$ ) and an outer probe located in the logarithmic region (here  $z_0^+ = 3.9Re_\tau^{1/2}$ ). The wall probe measures  $\tau$  by using the linear relationship between  $\tau$  and  $u$  in the viscous sublayer (Alfredsson *et al.* 1988). A schematic of the experimental setup is shown in figure 1. The wall probe is mounted over a glass plug in order to limit interference effects between the wall and the hot wire. This hot wire has been calibrated *in-situ*, directly in terms of  $\tau$ , using the asymptotic similarity formulations for  $Re_{\delta^*}$  versus  $Re_x$  as given by Monkewitz *et al.* (2007), and  $U_\tau$  versus  $Re_{\delta^*}$  as given by Nagib *et al.* (2009):

$$U_\tau = U_\infty \left( \frac{1}{\kappa} \ln(Re_{\delta^*}) + C_* \right)^{-1}, \quad (3.1)$$

where  $\kappa = 0.384$  and  $C_* = 3.3$ . The hot-wire outer probe is calibrated against a Pitot-static tube in the free-stream flow. Examples of fluctuating signals are given in figure 2, where a high degree of correlation between the outer-probe velocity signal and the wall-shear-stress signal can be observed. It should be noted that the size of the sensing length in viscous wall units,  $l^+ = 11.5$ , used for the calibration measurements (table 1) may not be small enough to adequately resolve the smallest scales. Smits *et al.* (2011b) suggested that in the viscous sublayer a sensing

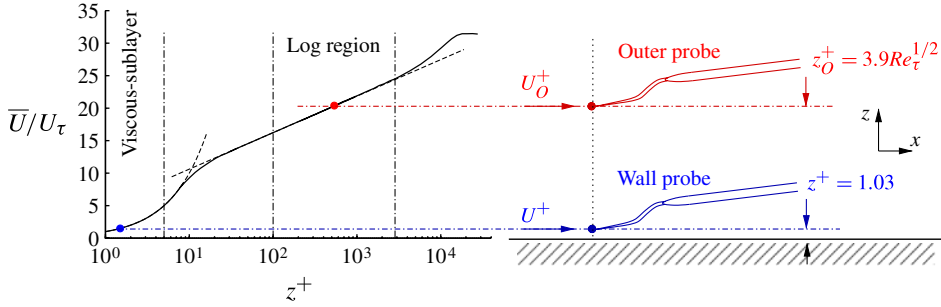


FIGURE 1. (Colour online) Experimental setup featuring the two-point simultaneous hot-wire measurements for the calibration of the model. The wall probe is mounted in the viscous sublayer at  $45\ \mu\text{m}$  above the wall ( $z^+ = 1.03$ ), and the outer probe is positioned at the geometric centre of the logarithmic region  $z_0^+ = 3.9Re_\tau^{1/2}$ .

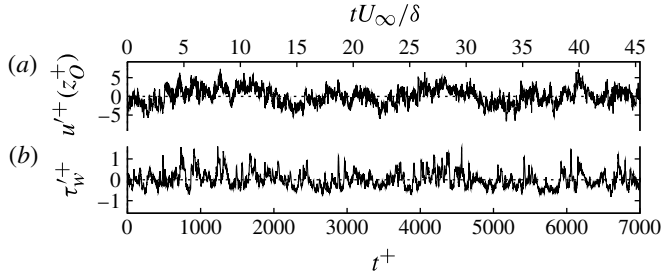


FIGURE 2. Example of fluctuating signals for  $Re_\tau = 4480$ : (a) raw fluctuating streamwise velocity component at  $z_0^+ = 3.9Re_\tau^{1/2}$ ; and (b) raw fluctuating wall shear stress.

length  $l^+ < 5$  is necessary to capture all the energy-containing events. However, the characteristics of the measured  $\tau_w$ -signal have all the features that have previously been reported in the literature:  $\tau_{w,rms}^+ \simeq 0.4$ , skewness of 1.0 and kurtosis of 4.78 as shown in figure 3(b) (see Örlü & Schlatter 2011). Furthermore, the cross-correlation profile between the  $\tau_w$ - and  $u$ -signals, shown in figure 3(a) by the solid line, is found to be consistent with the expected trend based on previous studies (Marusic & Heuer 2007).

To validate the model we use a series of datasets previously reported by Kulandaivelu (2012). These consist of a range of Reynolds numbers between  $Re_\tau \simeq 2700$  and 23 000 (see table 2). In addition, a very-high-Reynolds-number dataset is also used to infer the indicative asymptotic Reynolds number trend. These data are from the atmospheric surface layer (ASL) measured at the SLTEST facility in the Great Salt Lake Desert in Western Utah, as described by Marusic & Heuer (2007). A full description of the facility and measurement procedure is available in Klewicki *et al.* (1995), Metzger & Klewicki (2001) and Kunkel & Marusic (2006). Despite the field measurement uncertainties, the SLTEST results have been found to agree well with boundary layer data from laboratory facilities (Hutchins & Marusic 2007a; Marusic & Heuer 2007; Marusic & Hutchins 2008; Hutchins *et al.* 2012).

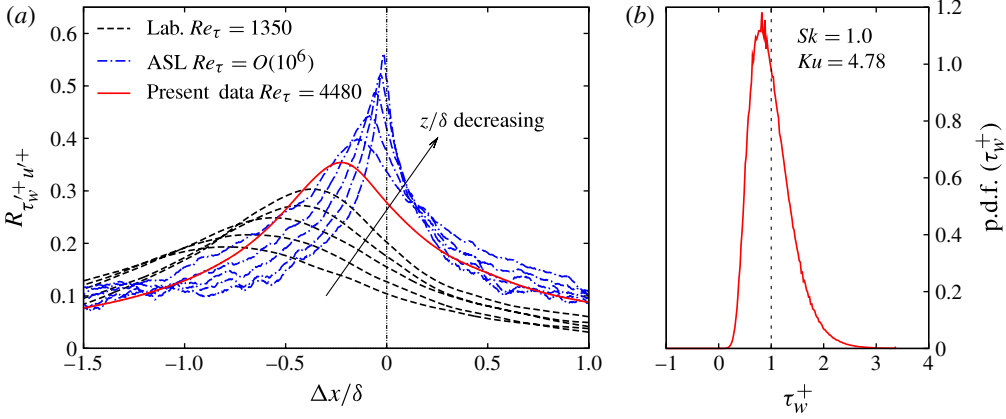


FIGURE 3. (Colour online) (a) Cross-correlation coefficient between  $\tau_w^+$  and  $u^+$  of the calibration experiment. Here,  $\Delta x = \Delta t U_c$  using Taylor's hypothesis where the convection velocity is  $U_c = U(z_0^+)$ . Dot-dashed lines (blue online) are from ASL measurements at  $Re_\tau = O(10^6)$  (Marusic & Heuer 2007) for  $z/\delta = 0.0024, 0.005, 0.0091, 0.0165$  and  $0.0293$ . Solid line (red online) is for present data at  $Re_\tau = 4480$  for  $z/\delta = 0.058$ . Dashed black lines correspond to laboratory wind tunnel results (Marusic, Kunkel & Porté-Agel 2001; Kunkel & Marusic 2003) at  $Re_\tau = 1350$  for  $z/\delta = 0.073, 0.091, 0.115, 0.145$  and  $0.183$ . (b) Probability density function of the total wall shear stress  $\tau_w^+$  of the calibration measurements, for the skewness and kurtosis values shown. The vertical dashed line marks the mean value  $\tau_w^+$ .

#### 4. Calibration of the model

Following the model of Marusic *et al.* (2010b), the parameters  $\tau_w^{/*}$ ,  $\alpha$  and  $\beta$  of the model given in (2.1) are obtained from a calibration experiment, conducted at  $Re_\tau = 4480$  (see figure 1 and table 1), from which  $\tau_w^{'+}$  ( $= \tau_{wp}^{'+}$  in (2.1)) and  $u_{OL}^{'+}$  are simultaneously known. The first step of the calibration is to remove the large-scale contribution from the wall-shear-stress signal. Hence, both signals  $\tau_w^{'+}$  and  $u^{'+}(z_0^+)$  are high-pass filtered at a cut-off frequency  $f^+ = 2.65 \times 10^{-3}$  (which is equivalent to  $\lambda_x^+ = 7000$  as was used by Mathis *et al.* 2011a for this calibration experiment), to retain their large-scale components  $\tau_{wL}^{'+}$  and  $u_L^{'+}(z_0^+)$ . (See Mathis *et al.* 2009a and Mathis *et al.* 2011a for further details about the choice of the cut-off wavelength for distinguishing small from large scales.)

From this, using the cross-correlation between these two filtered signals, we can determine the coefficient of superposition  $\alpha$ , and the large-scale structural angle  $\theta_L$ , such that

$$\alpha = \max(R_{\tau_{wL}^{'+} u_{OL}^{'+}}) \frac{\sqrt{\tau_{wL}^{'+2}}}{\sqrt{u_{OL}^{'+2}}}, \quad (4.1)$$

and

$$\theta_L = \arctan \frac{\Delta z}{\Delta x_m}, \quad (4.2)$$

where  $\Delta z^+ = z_0^+ - z^+ \simeq 3.9 Re_\tau^{1/2} - 1$ , and  $\Delta x_m$  corresponds to the streamwise shift at the maximum of the correlation. Here, Taylor's hypothesis is used to convert time to streamwise distance using a convection velocity  $U_c^+ = U^+(z_0^+)$ , i.e. the mean velocity

at the outer location. This choice of convection velocity is supported by the study of Hutchins *et al.* (2011), who used a streamwise spatial array of skin-friction sensors to detect the convection velocity of the large-scale-motion footprint at the wall, and found that it closely matched the mean velocity in the logarithmic region at  $z_0^+$ .

The coefficient  $\alpha$  corresponds to the maximum of the cross-correlation  $R_{\tau_w^+ u_L^+}$ , which is multiplied by the ratio of the r.m.s. values of the large-scale components to account for the combination of two signals having fluctuations of different orders of magnitude. This coefficient is found to be  $\alpha = 0.0898$ . The mean inclination angle, found to be  $\theta_L = 14.1^\circ$ , is used to form the log-region time-series signature of the large scales,  $u_{OL}^+$ , by shifting the filtered outer signal  $u_L^+(z_0^+)$  forward in the streamwise direction:

$$u_{OL}^+(t^+) = u_L^+(t^+ + U_c \Delta x_m, z_0^+). \quad (4.3)$$

With the coefficient of superposition  $\alpha$  and the large-scale signature  $u_{OL}^+$  now known, the large-scale trend, or the mean shift, imposed by the large-scale log-region events can be removed from the wall-shear-stress signal:

$$\tau_{wd}^+(t^+) = \tau_w^+(t^+) - \alpha u_{OL}^+(t^+), \quad (4.4)$$

where  $\tau_{wd}^+$  is the ‘de-trended’ signal.

With  $\alpha$ ,  $u_{OL}^+$  and  $\tau_{wd}^+$  determined, the remaining unknown parameters in (2.1) are the modulation parameter  $\beta$  and the universal signal  $\tau_w^{/*}$ . Combining (4.4) with (2.1) gives

$$\tau_{wd}^+(t^+) = \tau_w^{/*}(t^+) \{1 + \beta u_{OL}^+(t^+)\}. \quad (4.5)$$

Hence,  $\beta$  and  $\tau_w^{/*}$  are found using an iterative procedure for a solution of (4.5) that gives a non-amplitude-modulated universal signal (we recall that  $\tau_w^{/*}$  is defined to be a statistically ‘universal’ wall-shear-stress signal that would exist in the absence of large-scale effects, i.e. no superposition or modulation effects):

$$\tau_w^{/*}(t^+) = \frac{\tau_{wd}^+(t^+)}{1 + \beta u_{OL}^+(t^+)}, \quad \beta \text{ such as } \text{AM}(\tau_w^{/*}) = 0, \quad (4.6)$$

where  $\text{AM}(\tau_w^{/*})$  is the degree of amplitude modulation of the universal signal by the large-scale log-region events  $u_{OL}^+$ , as given by Mathis *et al.* (2009a). From this we find  $\beta = 0.0796$ . The pre-multiplied energy spectrum of the universal signal  $\tau_w^{/*}$  is shown in figure 4, along with the original measured signal. It is noted that the universal signal has most of its large-scale, low-frequency, content removed. Such behaviour was expected since the calibration procedure aims to remove the large-scale influence, leading to a statistically representative wall-shear-stress signal,  $\tau_w^{/*}$ , that would exist in the absence of large-scale motions. Thus,  $\tau_w^{/*}$  is a characteristic small-scale signal defined as universal in the sense that it is Reynolds-number independent.

## 5. Quasi-steady description of the inner-outer interaction

Before further describing the model, it is worthwhile considering the problem from a theoretical point of view, simplified by the boundary conditions created at the wall. The classical view on the universality of near-wall turbulence is that all the flow variables, if expressed in wall units, are independent of the Reynolds number. Thus, for the skin friction  $\tau_w$  this means

$$\tau_w = \tau_0 \tau_w^*(t^+) = \tau_0 \tau_w^*(t\tau_0/\mu), \quad (5.1)$$



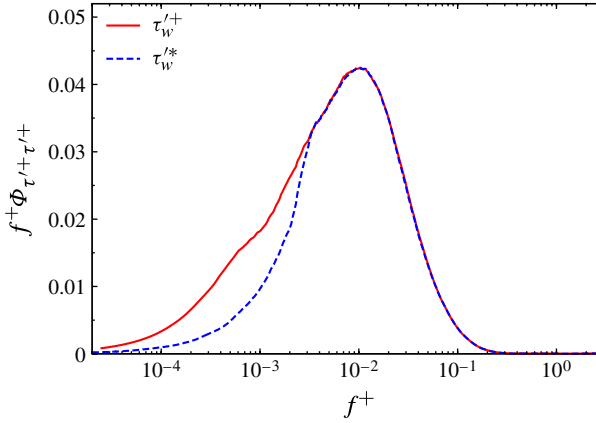


FIGURE 4. (Colour online) Pre-multiplied energy spectra of the original wall shear stress  $\tau_w^{'+}$  for  $Re_\tau = 4480$ , and the universal wall-shear-stress signal  $\tau_w^{/'*}$ .

where  $\tau_0 = \bar{\tau}_w = \rho U_\tau^2$  is the mean skin friction,  $\mu$  is the dynamic viscosity, and  $\tau_w^*(t^+)$  would be a universal function with all its statistics independent of  $Re$ , and its time average equal to one,  $\bar{\tau}_w^* = 1$ . (It should be noted that all the quantities here are the total values, while fluctuations are explicitly marked with a prime and time-average values with an overbar.)

The experimentally observed effect of large-scale structures on the near-wall turbulence is in contradiction with (5.1). We propose therefore to replace (5.1) with a model recognizing a quasi-steady character of the dependence of the skin friction on the large-scale effects.

To do this we suppose that the near-wall turbulence is universal, but it is affected by slowly varying outer structures and, hence,  $\tau_0$  is slowly varying with time:

$$\tau_0(t) = \bar{\tau}_0 + \tau_0'(t). \quad (5.2)$$

Then instead of (5.1) we have:

$$\tau_w = \tau_0(t) \tau_w^*(t \tau_0(t) / \mu). \quad (5.3)$$

Here,  $\tau_w^*$  remains a universal function of its argument, but it is amplitude-modulated by a large-scale, low-frequency varying signal. It is also frequency-modulated via a slowly varying factor in its argument. In general, this second effect might be important. However, when checked we found that it is quite weak as far as the comparisons and calibration procedures considered in the present work are concerned. For this reason we will neglect any frequency-modulation effect in what follows. Then (5.3) can be rewritten as

$$\tau_w = (\bar{\tau}_0 + \tau_0') \tau_w^*. \quad (5.4)$$

To compare this to the model (2.1), we can rewrite (5.4) in term of fluctuations

$$\tau_w = \bar{\tau}_w + \tau_w' \quad (5.5)$$

and

$$\tau_w^* = 1 + \tau_w^{/'*}. \quad (5.6)$$

Since the characteristic time scale of the large-scale structures is much greater than the characteristic time scale of the near-wall turbulence, it can be assumed that the large-scale fluctuations  $\tau'_0$  and the universal fluctuating component  $\tau_w'^*$  are uncorrelated, leading to  $\bar{\tau}_0 = \bar{\tau}_w$ . It should be noted that this assumption has been confirmed using the calibration dataset in table 1, in which we found  $\bar{\tau}'_0 \tau_w'^* \simeq 0$ . Substituting (5.5), (5.6), and  $\bar{\tau}_0 = \bar{\tau}_w$  into (5.4), neglecting the nonlinear fluctuation terms, and rearranging gives

$$\tau_w'^+ = \frac{\tau'_0}{\bar{\tau}_w} = \tau_w'^* \left( 1 + \frac{\tau'_0}{\bar{\tau}_w} \right) + \frac{\tau'_0}{\bar{\tau}_w}. \quad (5.7)$$

Comparing this with the wall-shear-stress predictive model given in (2.1), which has the form

$$\tau_{wp}'^+ = \tau_w'^*(1 + \beta u_{OL}'^+) + \alpha u_{OL}'^+, \quad (5.8)$$

where  $u_{OL}'^+$  is the fluctuating large-scale signal from the log region, one can see that if the modulation effect is quasi-steady and the fluctuations are small enough to neglect the nonlinear terms then

$$\frac{\tau'_0}{\bar{\tau}_w} = \alpha u_{OL}'^+ \quad (5.9)$$

and

$$\frac{\tau'_0}{\bar{\tau}_w} = \beta u_{OL}'^+, \quad (5.10)$$

that is,  $\alpha$  and  $\beta$  should be equal. In the calibration of the model in § 4 these quantities were found independently from the experiment using a very different procedure, and we found that  $\alpha = 0.0898$  and  $\beta = 0.0796$ . The small difference between these values gives the first confirmation of our interpretation of the modulation effect. It is noted that the procedure for determining  $\beta$  relies on a choice of scheme to quantify the degree of amplitude modulation, which results in variations in the precise value of  $\beta$  depending on the adopted scheme (some alternatives have been recently discussed by Schlatter & Örlü 2010, Bernardini & Pirozzoli 2011 and Mathis *et al.* 2011a,b). The theoretical arguments that lead to  $\alpha = \beta$  are preferred as they involve fewer assumptions.

## 6. New calibration method

Based on the theoretical basis developed above, the model is simplified and recalibrated assuming that the coefficients of superposition  $\alpha$  and modulation  $\beta$  are identical. Therefore, (2.1) becomes:

$$\tau_{wp}'^+(t^+) = \tau_w'^*(t^+) \{ 1 + \alpha u_{OL}'^+(t^+) \} + \alpha u_{OL}'^+(t^+), \quad (6.1)$$

where now only two unknown quantities appear ( $\alpha$  and  $\tau_w'^*(t^+)$ ). Here, the same procedure as used in § 4 is applied to determine the coefficient  $\alpha$ , the large-scale structural angle  $\theta_L$ , and to form the log-region time-series signature of the large scales  $u_{OL}'^+$ . Once these parameters are determined, the new universal signal  $\tau_w'^*(t^+)$  is found by simply solving (6.1):

$$\tau_w'^*(t^+) = \frac{\tau_w'^+(t^+) - \alpha u_{OL}'^+(t^+)}{1 + \alpha u_{OL}'^+(t^+)}, \quad (6.2)$$

where  $\tau_w'^+(t^+)$ ,  $u_{OL}'^+$  and  $\alpha = 0.0898$  are simultaneously known.

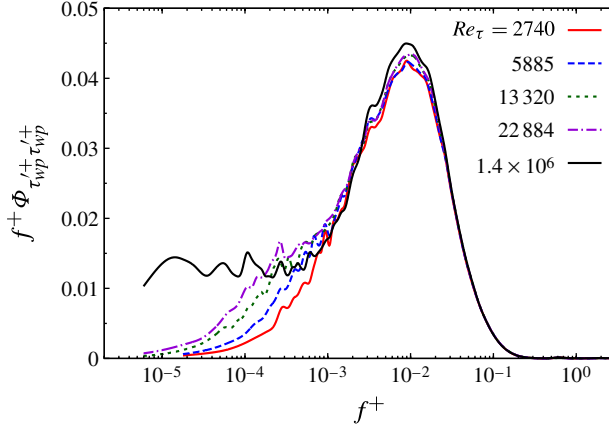


FIGURE 5. (Colour online) Reynolds number trend of the pre-multiplied energy spectra of the predicted wall-shear-stress signal.

## 7. Predictions

With all parameters of the model being calibrated, i.e.  $\tau_w^*$ ,  $\alpha$  and  $\theta_L$ , the predictive model can now be used to reconstruct a statistically representative wall-shear-stress signal  $\tau_{wp}^{\prime+}$  at any Reynolds number, using (6.1) and provided only the corresponding large-scale signal  $u_{OL}^{\prime+}$ . The measured log-region signal,  $u^{\prime+}(z_O^+)$ , is taken at the same wall-normal location  $z_O^+$  used during the calibration. It should be emphasized that this signal does not require a fully spatially resolved measurement, but it does require information for structures with a non-dimensional frequency of  $f^+ < 2.65 \times 10^{-3}$ . The large-scale signal  $u_{OL}^{\prime+}$  is then obtained using (4.3).

Below, we present shear-stress predictions from measurements in the logarithmic region for the datasets given in table 2, which cover a large range of Reynolds numbers, from  $Re_\tau \simeq 2700$  to  $1.4 \times 10^6$ .

The pre-multiplied energy spectra of the predicted wall-shear-stress signals,  $k_x \Phi_{\tau_{wp}^{\prime+} \tau_{wp}^{\prime+}}$ , are shown in figure 5 for several Reynolds numbers. Though no experimental data are available for comparison, it can be seen that the model captures well the overall Reynolds number trend, i.e. a slight increase with  $Re_\tau$  of the large-scale energy content. This behaviour agrees well with recent understanding of Reynolds number effects in the turbulent boundary layer, which are now well established to be closely related to the strengthening of the large scales with  $Re$  (Townsend 1976; Adrian *et al.* 2000; Metzger & Klewicki 2001; del Álamo *et al.* 2004; Marusic *et al.* 2010a, and others). The increase in the energy contained in the long wavelengths also suggests an increase in the r.m.s. of  $\tau_w^{\prime+}$ . This is well supported by figure 6 which shows the fluctuation magnitude of the predicted wall-shear-stress signal,  $\sqrt{\tau_{wp}^{\prime+2}}$ , as a function of the Reynolds number. Also included in this figure are available data for a flat-plate zero-pressure-gradient turbulent boundary layer from Österlund (1999), Komminaho & Skote (2002) and Schlatter & Örlü (2010). The overall Reynolds number trend of  $\sqrt{\tau_{wp}^{\prime+2}}$  appears to be correctly captured by the model, and it is in good agreement with the recent work of Örlü & Schlatter (2011). They reported that  $\sqrt{\tau_{wp}^{\prime+2}}$  increases slowly with Reynolds number, and they attributed

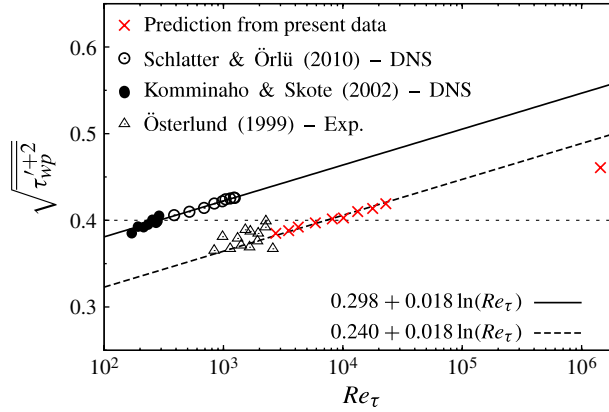


FIGURE 6. (Colour online) Fluctuation magnitude of the wall shear stress  $\sqrt{\tau_{wp}^{'+2}}$  versus Reynolds number  $Re_\tau$ , for the prediction, and available data for a zero-pressure-gradient turbulent boundary layer. The solid line indicates the Reynolds number trend reported by Schlatter & Örlü (2010)  $\sqrt{\tau_{wp}^{'+2}} = 0.298 + 0.018 \ln(Re_\tau)$ . The dashed sloping line indicates the trend  $\sqrt{\tau_{wp}^{'+2}} = 0.240 + 0.018 \ln(Re_\tau)$ . The horizontal dashed line marks the classical value of 0.4 suggested by Alfredsson *et al.* (1988).

this to the growing influence of the large scales (in contrast with the long-standing classical view of the constant value of 0.4 given by Alfredsson *et al.* 1988). However, the predictions show an overall underestimation of  $\sqrt{\tau_{wp}^{'+2}}$ . An application of the correction scheme of Smits *et al.* (2011b) demonstrates that this discrepancy is only partially attributable to spatial resolution effects due to the finite size of the hot-wire sensor used in the calibration measurements ( $l^+ = 11.5$ ). Hot-wire measurements very close to the wall will also experience heat transfer between the probe and the wall, reducing the measured signal intensity (Bruun 1995; Chew *et al.* 1998). This seems to be the more significant cause of the discrepancy in this case. Nevertheless, the correctly predicted Reynolds number trend in  $\sqrt{\tau_{wp}^{'+2}}$  gives a good indication of the capabilities of the model, which are only dependent on the quality of the calibration measurements.

It is worth noting that the input of the wall-shear-stress model,  $u_{OL}^+$ , remains exactly the same as the input for the velocity model proposed previously (Marusic *et al.* 2010b; Mathis *et al.* 2011a). The robustness or insensitivity of the predictions to variations in the input signal (e.g. to the choice of cutoff filter used to extract  $u_{OL}^+$  or the precise log-region location where this signal is acquired) are the same for both models, and this has been well documented in Mathis *et al.* (2011a) and Inoue *et al.* (2012).

## 8. Predictions based on model calibrated using DNS dataset

As seen in figure 6, the present model, calibrated using experimental measurements, underestimates the wall-shear-stress intensity. This is probably due to spatial resolution effects and also heat loss to the substrate (Bruun 1995) which could be overcome by making a new calibration measurement using smaller sensors. However, a calibration

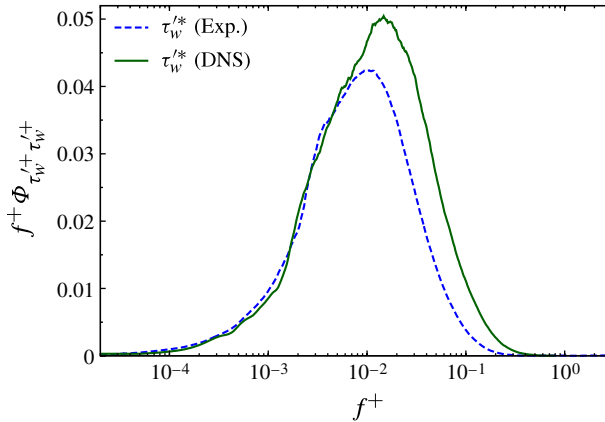


FIGURE 7. (Colour online) Pre-multiplied energy spectra of the universal wall-shear-stress signal  $\tau_w^{/*}$  obtained using experimental and DNS datasets.

measurement using a sufficiently small hot-wire sensor to avoid spatial resolution effects remains a challenging experiment, both in terms of feasibility and reliability. To address this problem, the wall-shear-stress model was re-calibrated using the DNS dataset of del Álamo *et al.* (2004) at  $Re_\tau = 934$ , which has an equivalent spatial resolution of  $l^+ = 3.8$ . The use of DNS data is justified based on the observation that the small-scale near-wall motions are very similar across all smooth wall-bounded turbulence, regardless of the flow geometry and large-scale content (e.g. pipe, channel or boundary layer, see Jiménez & Pinelli 1999; Schoppa & Hussain 2002; Monty *et al.* 2009, among others). In addition, a very similar superposition and amplitude modulation effect is also observed in all of these flows (Hutchins & Marusic 2007b; Monty *et al.* 2009; Mathis *et al.* 2009b). Under this assumption, the primary difference between turbulent pipe, channel and boundary layer flows lies only in the large scales (which are geometry specific). Since this information will be removed during the process of extracting the universal wall shear stress, the universal parameters can, in theory, then be extracted from any smooth wall-bounded flow with zero or weak pressure gradient.

The spatial wall-shear-stress DNS data are converted to a time-series using Taylor's hypothesis taking  $f = 12.1U_\tau/\lambda_x$ , as proposed by Kreplin & Eckelmann (1979). From this calibration new parameters  $\alpha$ ,  $\theta_L$  and  $\tau_w^{/*}$  were obtained. The new values for the constants are  $\alpha = 0.0989$  and  $\theta_L = 14.8$ . The corresponding pre-multiplied energy spectrum of the universal signal  $\tau_w^{/*}$  is shown in figure 7, along with the previous result from the experimental calibration measurement. The effect of the attenuation for the wall wire is clearly visible at the higher frequencies ( $f^+ \gtrsim 10^{-2}$ ), whereas a very good agreement is observed at the lower frequencies. This suggests the reliability of the calibration procedure using low-Reynolds-number data. (One might have suspected that the limited scale separation between small- and large-scale features might be a limiting factor for this technique at low  $Re$ ).

The fluctuation magnitude of the predicted wall-shear-stress signal using the DNS calibration is shown in figure 8, along with results from the literature. The  $Re$  trend is seen to be captured very well. These results show that the accuracy of the predictions relies on the quality of the dataset used to calibrate the model. In situations where the measured fluctuating wall shear stress is attenuated (by spatial resolution, heat

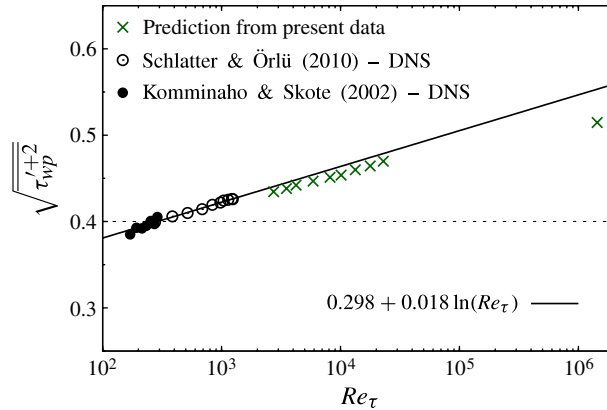


FIGURE 8. (Colour online) Fluctuation magnitude of the wall shear stress  $\sqrt{\tau_{wp}'^{+2}}$  versus Reynolds number  $Re_\tau$ , for the prediction based on calibration with DNS data, and available data for a zero-pressure-gradient turbulent boundary layer. The solid line indicates the Reynolds number trend reported by Schlatter & Örlü (2010)  $\sqrt{\tau_{wp}'^{+2}} = 0.298 + 0.018 \ln(Re_\tau)$ . The horizontal dashed line marks the classical value of 0.4 suggested by Alfredsson *et al.* (1988).

conduction to the wall, or aerodynamic interference effects) one can expect the model to give lower predictions.

## 9. Conclusions

In this paper, we have proposed a model that is able to reconstruct a realistic wall-shear-stress time-series signal for the smooth-wall zero-pressure-gradient turbulent boundary layer. To reconstruct the wall-shear-stress signal at any Reynolds number, the model requires only a signal of the large scales from the logarithmic region. The model has been built upon the recent model developed by Marusic *et al.* (2010b) and Mathis *et al.* (2011a) for the streamwise velocity component. The underlying idea is that the near-wall small-scale structures are universal, and the Reynolds number effects are modelled through an inner–outer interaction consisting of superposition and modulation effects of the large scales on the small scales. In addition, a theoretical description of the influence of the large-scale motions on the near-wall turbulence has allowed us to refine the mathematical formulation of the wall-shear-stress model. In the theoretical description the inner–outer interaction is described as a quasi-steady response of the near-wall turbulence to slow, large-scale variations of the skin friction. A low-frequency fluctuation is then added to the mean skin friction, which manifests itself both in modulation and superposition effects. The theoretical formulation, written in terms of fluctuations, coincides well with the empirical formulation, which has led us to identify that the coefficients of superposition and modulation should be identical in the wall-shear-stress model’s formulation. This allows us to reduce the number of parameters, resulting in a new procedure to calibrate the model. The model is shown to predict reasonably well the Reynolds number-dependence of the wall-shear-stress fluctuation magnitude, which is in good agreement with recent results (Örlü & Schlatter 2011). Furthermore, it is shown that the accuracy of the results is dependent on the spatial resolution of the calibration measurements, which does not

affect the Reynolds number trend. Hence, DNS data seem to be the most reliable data for calibrating the model as they provide accurate wall-shear-stress information with minimal spatial resolution effects, whereas near-wall experimental measurements remain highly challenging.

The present model is desirable for many practical problems related to turbulent boundary layers, where wall-shear-stress information is inaccessible or inaccurate but a low-frequency velocity signal away from the wall is available. For example, this could be useful in large-eddy simulations where only large-scale information above the near-wall region is available. The present model could be used to refine the near-wall models employed. In flow control applications, such as drag reduction, the wall-shear-stress model would be valuable to assess the efficiency of the control device in affecting the skin friction. Finally, in environmental studies, such as on the atmospheric surface layer, or a stream or river, the near-wall region is largely inaccessible, and the present wall-shear-stress model could possibly constitute a valuable tool to complete and enhance the reliability of the field measurements. It is emphasized that the model has thus far only been calibrated and validated for flat-plate smooth-wall flows, and the model's parameters would strictly need to be re-calibrated for the appropriate roughness and pressure-gradient conditions for the given application. Given the highly challenging nature of accurate experimental measurements of friction velocity and fluctuating wall shear stress in rough-wall and pressure-gradient boundary layers, it seems likely that DNS may provide the most feasible and reliable way of calibrating the universal parameters of the model in these cases.

### Acknowledgements

The authors wish to thank Dr V. Kulandaivelu for assisting in the experiments, and gratefully acknowledge the Australian Research Council for its financial support. The third author gratefully acknowledges the financial support from EPSRC through grant EP/G060215/1, together with Airbus Operations Ltd and EADS UK Ltd.

### REFERENCES

- ADRIAN, R. J., MEINHART, C. D. & TOMKINS, C. D. 2000 Vortex organization in the outer region of the turbulent boundary layer. *J. Fluid Mech.* **422**, 1–54.
- DEL ÁLAMO, J. C. & JIMÉNEZ, J. 2003 Spectra of the very large anisotropic scales in turbulent channels. *Phys. Fluids* **15** (6), L41–L44.
- DEL ÁLAMO, J. C., JIMÉNEZ, J., ZANDONADE, P. & MOSER, R. D. 2004 Scaling of the energy spectra of turbulent channels. *J. Fluid Mech.* **500**, 135–144.
- ALFREDSSON, P. H., JOHANSSON, A. V., HARITONIDIS, J. H. & ECKELMANN, H. 1988 The fluctuating wall-shear stress and the velocity-field in the viscous sublayer. *Phys. Fluids* **31** (5), 1026–1033.
- BANDYOPADHYAY, P. R. & HUSSAIN, A. K. M. F. 1984 The coupling between scales in shear flows. *Phys. Fluids* **27** (9), 2221–2228.
- BERNARDINI, M. & PIROZZOLI, S. 2011 Inner/outer layer interactions in turbulent boundary layers: a refined measure for the large-scale amplitude modulation mechanism. *Phys. Fluids* **23**, 061701.
- BRAND, A., LACY, J. R., HSU, H., HOOVER, D., GLADDING, S. & STACEY, M. T. 2010 Wind-enhanced resuspension in the shallow waters of South San Francisco Bay: mechanisms and potential implications for cohesive sediment transport. *J. Geophys. Res. – Oceans* **115**, 1–15.
- BROWN, G. L. & THOMAS, A. S. W. 1977 Large structure in a turbulent boundary-layer. *Phys. Fluids* **20** (10), S243–S251.

- BRUUN, H. H. 1995 *Hot-wire Anemometry*. Oxford University Press.
- CHAUHAN, K. A., NG, H. C. H. & MARUSIC, I. 2010 Empirical mode decomposition and Hilbert transforms for analysis of oil-film interferograms. *Meas. Sci. Technol.* **21**, 105404.
- CHEW, Y. T., KHOO, B. C., LIM, C. P. & TEO, C. J. 1998 Dynamic response of a hot-wire anemometer. Part II: a flush-mounted hot-wire and hot-film probes for wall shear stress measurements. *Meas. Sci. Technol.* **9**, 764–778.
- CHUNG, D. & MCKEON, B. J. 2010 Large-eddy simulation of large-scale structures in long channel flow. *J. Fluid Mech.* **661**, 341–364.
- DENNIS, D. J. C. & NICKELS, T. B. 2011a Experimental measurement of large-scale three-dimensional structures in a turbulent boundary layer. Part 1: vortex packets. *J. Fluid Mech.* **673**, 180–217.
- DENNIS, D. J. C. & NICKELS, T. B. 2011b Experimental measurement of large-scale three-dimensional structures in a turbulent boundary layer. Part 2: long structures. *J. Fluid Mech.* **673**, 218–244.
- FERNHOLZ, H. H. & FINLEY, P. J. 1996 The incompressible zero-pressure-gradient turbulent boundary layer: an assessment of the data. *Prog. Aerosp. Sci.* **32**, 245–311.
- GRANT, S. B. & MARUSIC, I. 2012 Crossing turbulent boundaries: interfacial flux in environmental flows. *Environ. Sci. Technol.* **45**, 1443–1453.
- GRANT, W. D. & MADSEN, O. S. 1986 The continental-shelf bottom boundary layer. *Annu. Rev. Fluid Mech.* **18**, 265–305.
- GRINVALD, D. & NIKORA, V. 1988 *Rechnaya Turbulentsiya (River Turbulence)*. Hydrometeoizdat (in Russian).
- HAMBLETON, W. T., HUTCHINS, N. & MARUSIC, I. 2006 Simultaneous orthogonal-plane particular image velocimetry measurements in turbulent boundary layer. *J. Fluid Mech.* **560**, 53–64.
- HUNT, J. C. R. & DURBIN, P. A. 1999 Perturbed vortical layers and shear sheltering. *Fluid Dyn. Res.* **24**, 375–404.
- HUNT, J. C. R., EAMES, I., WESTERWEL, J., DAVIDSON, P. A., VOROPAYEV, S., FERNANDO, J. & BRAZA, M. 2010 Thin shear layers – the key to turbulence structure? *J. Hydraul Environ. Res.* **4**, 75–82.
- HUNT, J. C. R. & MORRISON, J. F. 2000 Eddy structure in turbulent boundary layers. *Eur. J. Mech. (B/Fluids)* **19**, 673–694.
- HUTCHINS, N., CHAUHAN, K., MARUSIC, I., MONTY, J. P. & KLEWICKI, J. 2012 Towards reconciling the large-scale structure of turbulent boundary layers in the atmosphere and laboratory. *Boundary-Layer Meteorol.* **145**, 273–306.
- HUTCHINS, N. & MARUSIC, I. 2007a Evidence of very long meandering features in the logarithmic region of turbulent boundary layers. *J. Fluid Mech.* **579**, 1–28.
- HUTCHINS, N. & MARUSIC, I. 2007b Large-scale influences in near-wall turbulence. *Phil. Trans. R. Soc. Lond. A* **365**, 647–664.
- HUTCHINS, N., MONTY, J. P., GANAPATHISUBRAMANI, B., NG, H. C. H. & MARUSIC, I. 2011 Three-dimensional conditional structure of a high Reynolds number turbulent boundary layer. *J. Fluid Mech.* **673**, 255–285.
- HUTCHINS, N., NICKELS, T., MARUSIC, I. & CHONG, M. S. 2009 Spatial resolution issues in hot-wire anemometry. *J. Fluid Mech.* **635**, 103–136.
- INOUE, M., MATHIS, R., MARUSIC, I. & PULLIN, D. I. 2012 Inner-layer intensities for the flat-plate turbulent boundary layer combining a predictive wall-model with large-eddy simulations. *Phys. Fluids* **24** (7), 075102.
- JACOBS, R. G. & DURBIN, P. A. 1998 Shear sheltering and the continuous spectrum of the Orr-Sommerfeld equation. *Phys. Fluids* **10** (8), 2006–2011.
- JIMÉNEZ, J. & PINELLI, A. 1999 The autonomous cycle of near-wall turbulence. *J. Fluid Mech.* **389**, 335–359.
- KIM, K. C. & ADRIAN, R. J. 1999 Very large-scale motion in the outer layer. *Phys. Fluids* **11**, 417–422.
- KLEWICKI, J. C. 2010 Reynolds number dependence, scaling, and dynamics of turbulent boundary layers. *Trans. ASME: J. Fluids Engng* **132**, 094001.



- KLEWICKI, J. C., METZGER, M. M., KELNER, E. & THURLOW, E. M. 1995 Viscous sublayer flow visualizations at  $Re_\theta = 1\,500\,000$ . *Phys. Fluids* **7**, 857–963.
- KOMMINAHO, J. & SKOTE, M. 2002 Reynolds stress budgets in Couette and boundary layer flows. *Flow Turbul. Combust.* **68**, 167–192.
- KREPLIN, H. P. & ECKELMANN, H. 1979 Propagation of perturbations in the viscous sublayer and adjacent wall region. *J. Fluid Mech.* **95**, 305–322.
- KULANDAIVELU, V. 2012 Evolution and structure of zero pressure gradient turbulent boundary layer. PhD thesis, The University of Melbourne, Melbourne.
- KUNKEL, G. J. & MARUSIC, I. 2003 An approximate amplitude attenuation correction for hot-film shear stress sensors. *Exp. Fluids* **34**, 285–290.
- KUNKEL, G. J. & MARUSIC, I. 2006 Study of the near-wall-turbulent region of the high-Reynolds-number boundary layer using atmospheric flow. *J. Fluid Mech.* **548**, 375–402.
- LENAERS, P., LI, Q., BRETHOUWER, G., SCHLATTER, P. & ÖRLÜ, R. 2012 Rare backflow and extreme wall-normal velocity fluctuations in near-wall turbulence. *Phys. Fluids* **24**, 035110.
- LIGRANI, P. M. & BRADSHAW, P. 1987 Spatial resolution and measurement of turbulence in the viscous sublayer using subminiature hot-wire probes. *Exp. Fluids* **5**, 407–417.
- MARUSIC, I. & HEUER, W. D. C. 2007 Reynolds number invariance of the structure angle in wall turbulence. *Phys. Rev. Lett.* **99**, 114501.
- MARUSIC, I. & HUTCHINS, N. 2008 Study of the log-layer structure in wall turbulence over a very large range of Reynolds number. *Flow Turbul. Combust.* **81**, 115–130.
- MARUSIC, I., KUNKEL, G. J. & PORTÉ-AGEL, F. 2001 Experimental study of wall boundary conditions for large-eddy simulation. *J. Fluid Mech.* **446**, 309–320.
- MARUSIC, I., MATHIS, R. & HUTCHINS, N. 2010a High Reynolds number effects in wall turbulence. *Int. J. Heat Fluid Flow* **31** (3), 418–428.
- MARUSIC, I., MATHIS, R. & HUTCHINS, N. 2010b Predictive model for wall-bounded turbulent flow. *Science* **329** (5988), 193–196.
- MARUSIC, I., MATHIS, R. & HUTCHINS, N. 2011 A wall shear stress predictive model. *J. Phys.: Conf. Ser.* **318** (1), 012003. *Proceeding of the 13th European Turbulence Conference (ETC13)*, Warsaw, Poland, 12–15 September 2011.
- MARUSIC, I., MCKEON, B. J., MONKEWITZ, P. A., NAGIB, H. M., SMITS, A. J. & SREENIVASAN, K. R. 2010c Wall-bounded turbulent flows: recent advances and key issues. *Phys. Fluids* **22**, 065103.
- MATHIS, R., HUTCHINS, N. & MARUSIC, I. 2009a Large-scale amplitude modulation of the small-scale structures in turbulent boundary layers. *J. Fluid Mech.* **628**, 311–337.
- MATHIS, R., HUTCHINS, N. & MARUSIC, I. 2011a A predictive inner–outer model for streamwise turbulence statistics in wall-bounded flows. *J. Fluid Mech.* **681**, 537–566.
- MATHIS, R., MARUSIC, I., HUTCHINS, N. & SREENIVASAN, K. R. 2011b The relationship between the velocity skewness and the amplitude modulation of the small scale by the large-scale in turbulent boundary layers. *Phys. Fluids* **23** (12), 121702.
- MATHIS, R., MONTY, J., HUTCHINS, N. & MARUSIC, I. 2009b Comparison of large-scale amplitude modulation in turbulent boundary layers, pipes and channel flows. *Phys. Fluids* **21** (11), 111703.
- METZGER, M. M. & KLEWICKI, J. C. 2001 A comparative study of near-wall turbulence in high and low Reynolds number boundary layers. *Phys. Fluids* **13**, 692–701.
- MONKEWITZ, P. A., CHAUHAN, K. A. & NAGIB, H. M. 2007 Self-consistent high-Reynolds-number asymptotics for zero-pressure-gradient turbulent boundary layers. *Phys. Fluids* **19**, 115101.
- MONKEWITZ, P. A., CHAUHAN, K. A. & NAGIB, H. M. 2008 Comparison of mean flow similarity laws in zero pressure gradient turbulent boundary layers. *Phys. Fluids* **20**, 105102.
- MONTY, J. P., HUTCHINS, N., NG, H. C. H., MARUSIC, I. & CHONG, M. S. 2009 A comparison of turbulent pipe, channel and boundary layer flows. *J. Fluid Mech.* **632**, 431–442.
- MONTY, J. P., STEWART, J. A., WILLIAMS, R. C. & CHONG, M. S. 2007 Large-scale features in turbulent pipe and channel flows. *J. Fluid Mech.* **589**, 147–156.

- NAGIB, H., SMITS, A., MARUSIC, I. & ALFREDSSON, P. H. 2009 ICET – International collaboration on experiments in turbulence: coordinated measurements in high Reynolds number turbulent boundary layers from three wind tunnels. In *Bulletin of the 62nd Annual Division of Fluid Dynamics Meeting of the American Physical Society, Minneapolis, Minnesota, USA, Series II, Vol. 54, No. 19 Nov. 2009*. American Physical Society.
- NICKELS, T. B., MARUSIC, I., HAFEZ, S. & CHONG, M. S. 2005 Evidence of the  $k_1^{-1}$  law in high-Reynolds number turbulent boundary layer. *Phys. Rev. Lett.* **95**, 074501.
- ÖRLÜ, R. & SCHLATTER, P. 2011 On the fluctuating wall-shear stress in zero-pressure-gradient turbulent boundary layers. *Phys. Fluids* **23**, 021704.
- ÖSTERLUND, J. M. 1999 Experimental studies of zero pressure-gradient turbulent boundary layer. PhD thesis, KTH, Stockholm.
- PRANDTL, L. 1905 Über Flüssigkeits bewegung bei sehr kleiner Reibung. In *Verhaldlg III Int. Math. Kong.* (ed. A. Krazer). pp. 484–491. Teubner, (also available in translation as: Motion of fluids with very little viscosity).
- PERRY, A. E. & MARUSIC, I. 1995 A wall-wake model for the turbulence structure of boundary layers Part 1. Extension of the attached eddy hypothesis. *J. Fluid Mech.* **298**, 361–388.
- PTASINSKI, P. K., BOERSMA, B. J., NIEUWSTADT, F. T. M., HULSEN, M. A., VAN DEN BRULE, B. H. A. A. & HUNT, J. C. R. 2003 Turbulent channel flow near maximum drag reduction: simulations, experiments and mechanisms. *J. Fluid Mech.* **490**, 251–291.
- ROWIŃSKI, P., ABERLE, J. & MAZURCZYK, A. 2005 Shear velocity estimation in hydraulic research. *Acta Geophys. Pol.* **53** (4), 567–583.
- SCHLATTER, P. & ÖRLÜ, R. 2010 Assessment of direct numerical simulation data of turbulent boundary layer. *J. Fluid Mech.* **659**, 116–126.
- SCHLATTER, P. & ÖRLÜ, R. 2010 Quantifying the interaction between large and small scales in wall-bounded turbulent flows: a note of caution. *Phys. Fluids* **22** (5), 051704.
- SCHLICHTING, H. & GERSTEN, K. 2000 *Boundary Layer Theory*, 8th revised and enlarged edn. Springer.
- SCHOPPA, W. & HUSSAIN, F. 2002 Coherent structure generation in near-wall turbulence. *J. Fluid Mech.* **453**, 57–108.
- SMITS, A. J., MCKEON, B. J. & MARUSIC, I. 2011a High-Reynolds number wall turbulence. *Annu. Rev. Fluid Mech.* **43**, 353–375.
- SMITS, A. J., MONTY, J. P., HULTMARK, M., BAILEY, S. C. C., HUTCHINS, N. & MARUSIC, I. 2011b Spatial resolution correction for wall-bounded turbulence measurements. *J. Fluid Mech.* **676**, 41–53.
- TOMKINS, C. D. & ADRIAN, R. J. 2003 Spanwise structure and scale growth in turbulent boundary layers. *J. Fluid Mech.* **490**, 37–74.
- TOWNSEND, A. A. 1976 *The Structure of Turbulent Shear Flow*, 2nd edn. Cambridge University Press.
- ZAKI, T. & SAHA, S. 2009 On shear sheltering and the structure of vortical modes in single- and two-fluid boundary layers. *J. Fluid Mech.* **626**, 111–147.